In-Situ Observations of Martensitic Transformation in Blast-Resistant Steel

XINGHUA YU, SUDARSANAM SURESH BABU, JOHN C. LIPPOLD,
HIDENORI TERASAKI, and YU-ICHI KOMIZO

A hybrid *in-situ* characterization system, which couples the laser scanning confocal microscopy (LSCM) with the time-resolved X-ray diffraction (TRXRD) measurement with synchrotron radiation, was used to characterize the microstructure evolution during heat-affected zone (HAZ) thermal cycling of high-strength and blast-resistant steel. The combined technique has a time resolution of 0.3 seconds that allows for high-fidelity measurements of transformation kinetics, lattice parameters, and morphological features. The measurements showed a significant reduction in the martensite start transformation temperature with a decrease in the prior austenite grain size. In addition, the LSCM images confirmed the concurrent refinement of martensite packet size with smaller austenite grain sizes. This is consistent with dilatometric observations. The austenite grain size also influenced the rate of transformation (df_m/dT); however, the measurements from the hybrid (surface) and dilatometric (volume) measurements were inconsistent. Challenges and future directions of adopting this technique for comprehensive tracking of microstructure evolution in steels are discussed.

DOI: 10.1007/s11661-011-0746-4

I. INTRODUCTION

To meet the rigorous requirements for U.S. Navy hull and deck application, a blast-resistant steel, BlastAlloy 160 (BA-160, QuesTek Innovations LLC, Evanston, IL), was developed by Northwestern University researchers.[1,2] This steel is based on a low-carbon martensitic matrix that is strengthened by nanometer-sized Cu-rich precipitates and M_2C precipitates (where M = Cr, Mo, and V). The yield strength of BA-160 is 1104 MPa (160 ksi). The overarching goal of this development activity is to replace the currently certified high-strength low-alloy steels for use in surface ship structure. In order to meet this goal, the steel has to be weldable. Current research pertains to the on-going weldability research using small-scale samples. The activities include thermomechanical simulation, electron microscopy, and atom probe characterization, as well as thermodynamic and kinetic modeling of the microstructure evolution in the heat-affected zone (HAZ) region. The preceding data can be used to fine tune the base metal, as well as to design welding process parameters.

Prior research samples were subjected to thermal cycles typical of that of HAZ regions, with controlled heating rate, peak temperature (T_P), and cooling rates, in a GLEEBLE* thermomechanical simulator. No significant changes in microstructure and hardness were detected in the subcritical HAZ ($T_P < Ac_1$) samples. Some hardening was observed in the intercritical HAZ (ICHAZ, $Ac_1 < T_P < Ac_3$) samples. Softening was observed in samples subjected to fine-grained HAZ (FGHAZ, $T_P > Ac_3$) and coarse-grained HAZ (CGHAZ, $T_P >> Ac_3$) thermal cycles. Atom-probe tomography characterization and strength models correlated the softening to the dissolution of Cu precipitates and carbides.[3] In the next step, methodology to restore the strength, without any postweld heat treatment, was considered. One of the innovative approaches is to leverage repeated thermal cycles that may ensue during multipass welding. In agreement with this hypothesis, Cu reprecipitation and recovery of strength were observed after a double thermal cycles heat treatment.[4] The preceding studies also demonstrated that martensite substructure plays an important role in strengthening of BA-160.[3] For example, fine martensite substructure contributed to the hardening in the samples subjected to the intercritical HAZ thermal cycle. This was attributed to the reduced martensite plate/lath/packet size, which in turn is related to small austenite grain diameter. This observation is in agreement with the research of Morito *et al.*[5] The preceding microstructure evolutions were rationalized with *ex-situ* characterization tools including optical microscopy and electron backscattered diffraction imaging. However, to develop a comprehensive computational model for

---

*GLEEBLE is a trademark of Dynamic Systems Inc., Poestenkill, NY.

XINGHUA YU, Graduate Student, SUDARSANAM SURESH BABU, Associate Professor, and JOHN C. LIPPOLD, Professor, are with the Department of Materials Science and Engineering, The Ohio State University, Columbus, OH 43221. Contact e-mail: babu.13@osu.edu HIDENORI TERASAKI, Associate Professor, and YU-ICHI KOMIZO, Professor, are with JWRI, Osaka University, Osaka, Japan.

Manuscript submitted February 27, 2011.

HAZ, there is a need to measure the kinetics of microstructural evolution (fraction transformed and morphology) during continuous cooling conditions typical of that of welding. Although the dilatation measurements during GLEEBLE thermal simulation can be considered as an indirect *in-situ* measurement, the transients in morphological changes and crystallographic information are not accessible by this technique.

One of the *in-situ* approaches to investigate phase transformation in steels is laser scanning confocal microscopy (LSCM).[6–8] The LSCM system includes scanning optical microscopy and an infrared furnace. The surface of the samples can be imaged continuously while being subjected to a preprogrammed thermal cycle. The LSCM system was used to study the transformation kinetics of allotriomorphic ferrite,[9] to observe the solidification and ferrite to austenite transformation of high strengthened steel[10] and transformation kinetics from δ-ferrite to γ-austenite,[6] and to investigate the ferrite nucleation sites in weldments.[11] Though LSCM has the capacity of tracking real time morphology, the crystal structure information cannot be obtained. On the other hand, the time-resolved X-ray diffraction (TRXRD) technique is capable of characterizing the lattice parameter and volume fraction of phases (fcc and bcc) as a function of imposed thermal cycles. In the past decade, synchrotron-based *in-situ* TRXRD systems were used extensively to investigate phase transformations in steels.[12–17]

Considering the advantages of the LSCM and synchrotron TRXRD techniques, Komizo and Terasaki[18] developed a hybrid *in-situ* system that combines both methods. The current article uses this hybrid *in-situ* system to characterize martensitic transformation in BA-160 samples subjected to HAZ thermal cycles.

Phase transformation study by the high-speed X-ray diffraction technique using synchrotron radiation allows one to obtain the crystal structure information, such as lattice parameter, of all the phases presented in the sample, as well as their phase fractions (~0.01) under *in-situ* conditions. Moreover, changes in chemical composition of phases could be estimated from the lattice parameter data. For example, Babu *et al.*[15] derived carbon concentration in both austenite and ferrite during bainitic transformation in steel. However, analyzed volume by X-ray diffraction is indeed small and located on the top surface of the sample. Even though synchrotron radiation X-ray has a high penetration into materials, the volume analyzed is estimated to be on the order of 0.01 mm^3. The results will be biased if the sample contains large grain size due to free surface effects. The phase transformation can also be studied by measuring the relative length or radius change of the sample using a dilatometer. This is relevant to decomposition of austenite (fcc) to ferrite or martensite (bcc or bct) due to large differences in specific volume and the coefficient of thermal expansion. The volume analyzed in the dilatometer could be as large as several cubic millimeters. Since the dilatation is measured throughout the sample length or diameter, the results correspond to the average transformation behavior. Although the carbon concentration of austenite can be calculated from dilatometry data, however, the methodology requires the following assumptions:[19] (a) negligible change in coefficient of thermal expansion with temperature and (b) equilibrium carbon concentration in ferrite.

The transformation kinetics derived from synchrotron TRXRD are compared with dilatation study, as well as predictions from a martensite kinetics model. In this research, specific focus is given to the correlation between austenite grain size and martensite start temperature (M_s). Finally, some of the current challenges and future directions related to this hybrid technique are discussed.

II. EXPERIMENTAL

The chemical composition of the BA-160 is 0.06C, 6.8Ni, 1.9Cr, 0.61Mo, 0.015Si, 0.016Ti (wt pct), and the balance iron. Cylindrical samples were prepared with the dimension of 5 mm in diameter and 2 mm in height. The surfaces of the samples were final polished (0.02-μm colloidal silica) to be suitable for LSCM observation. Figure 1 shows the experimental setup of the hybrid *in-situ* observation system situated within a 46XU beam-

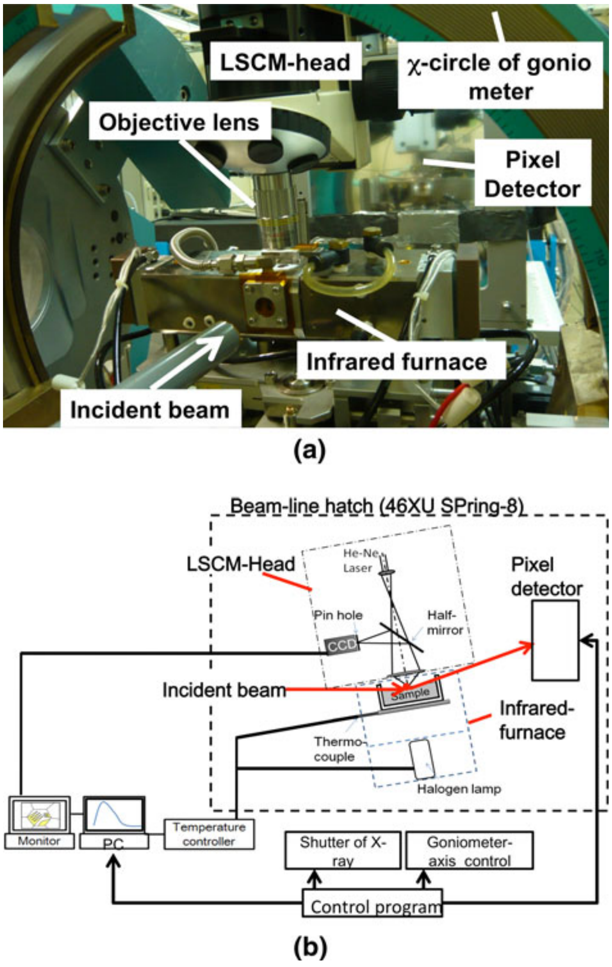

Fig. 1—Hybrid *in-situ* observation system: (*a*) photograph of the system at 46XU beamline at Spring-8; and (*b*) schematic illustration of the overall system with all the components.

line at Spring-8 (Hyogo, Japan). The infrared furnace was set on the theta-axis of the goniometer. The LSCM system containing a laser head and the furnace was attached to the theta-axis.

Samples were placed inside a boron nitride (BN) crucible, which was held by a platinum holder. A thermocouple was attached to the platinum holder to measure the temperature. The measured temperature was used to control the heat flux generated by the halogen lamps. The sample was placed at the focal point of the halogen lamp and mirror systems. During the experiments, the furnace was filled with pure argon (99.99996 pct) after evacuation to prevent oxidation. The LSCM recorded the images at a rate of 30 frames per second (time resolution = 0.03 seconds). The current work showed a small temperature gradient from the top to bottom of the sample, under rapid heating/cooling conditions. A correction factor was used to account for these gradients. The methodology for correcting the same and impact of temperature gradients on the accuracy of measurements will be discussed in Section III–E.

A large-area pixel detector, Pilatus 2M (DECTRIS Ltd., Baden, Switzerland),[20] was placed on the 2-theta-axis (Figure 1(a)). The incident beam (30 keV) shines on the sample surface placed in the furnace, and the resulting diffraction rings are recorded by the pixel detector. The time resolution X-ray diffraction (TRXRD) dictated by the detector hardware is 0.3 seconds. The X-ray with a wavelength was set at 0.413269 Å. The glancing angle of the beam on the sample surface was chosen to be 5 deg, and this leads to a total irradiated area on the sample surface of 2.07 mm^2 (Figure 1(b)). The depth of the X-ray interaction in the sample is estimated to be around ~16 μm.[18]

Three thermal cycles were selected (Figure 2) to simulate ICHAZ, FGHAZ, and CGHAZ regions. (1) In intercritical samples, the partial transformation of ferrite to austenite occurs. (2) In fine-grained HAZ samples, the peak temperature is slightly above the Ac_3 temperature, at which the complete transformation of ferrite to austenite occurs. (3) In the coarse-grained samples, the peak temperature is significantly above the Ac_3 temperature. The programmed heating rate and cooling rate were 293 K (20 °C)·s^{-1} and 283 K (10 °C)·s^{-1}, respectively.

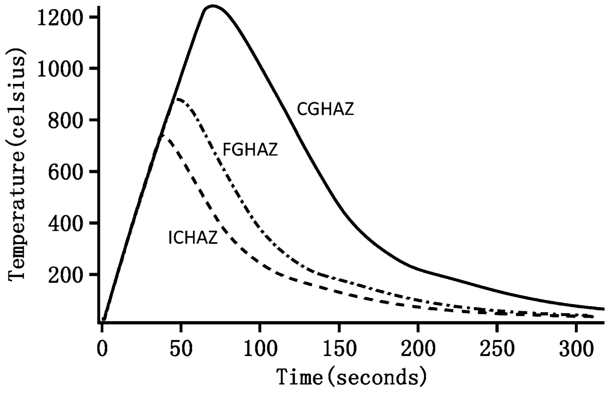

Fig. 2—Thermal cycles applied to simulate regions (ICHAZ, FGHAZ, and CGHAZ) of the HAZ with different peak temperatures are shown.

For each thermal cycle, 1000 diffraction images were collected from the pixel detector with a time resolution of 0.3 seconds. The diffraction rings on each image were integrated to give one-dimensional scans of intensity *vs* interplanar spacing.[21,22] In order to take care of possible changes in the incoming X-ray intensity, the diffraction intensity at each time interval was normalized with reference to the highest peak intensity. The diffraction data are then synchronized with measured thermal cycles. In the next step, the scans were analyzed by using automatic peak fitting algorithms. The methodologies for these are described in the published literature.[13,15]

In order to validate the preceding measurements, dilatation measurements were also made during similar thermal cycles. These experiments were performed separately using a GLEEBLE 3800 thermal-mechanical simulator. The dilatation measurements were made using a high-resolution dilatometer, on cylindrical samples (5-mm diameter and 73-mm length) along the radial direction. The sample temperature was controlled with a type-K thermocouple, which was wire percussion welded at the midsection very close to the dilatation measurements. The experiments were performed within a test chamber at an ambient pressure of 1.3 × 10^{-4} Pa (10^{-6} torr) to limit surface oxidation and thermocouple detachment.

III. RESULTS AND DISCUSSION

A. *Analysis of Transformation Kinetics by TRXRD*

Figure 3 shows two snapshots of X-ray diffraction rings recorded by the pixel detector. The images (CGHAZ sample) show the diffraction characteristics during heating at 1153 K and 1516 K (880 °C and 1243 °C).

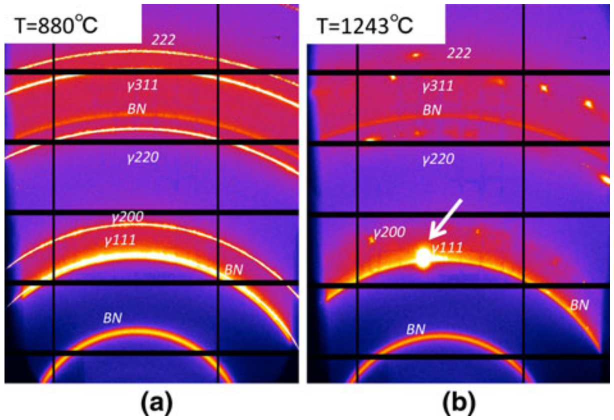

Fig. 3—Snapshots of images, showing diffraction rings, on heating the sample to different peak temperatures are shown. The dark bands are the region with no data due to the presence of masks. (*a*) On heating to 1153 K (880 °C), continuous rings are observed, indicating many small austenite grains that interact with the beam. (*b*) On heating to 1516 K (1243 °C), spotty features are observed due to the small number of large austenite grains that interact with the beam. These conditions lead to low SNR.

In both cases, the austenite is the only phase that is present in the sample. The data obtained at 1153 K (880 °C) show continuous diffraction rings from $\{111\}_{\text{fcc}}$ and $\{200\}_{\text{fcc}}$ lattice planes (Figure 3(a)). In contrast, the data obtained from 1516 K (1243 °C) show spotty diffraction images from the same and other lattice planes. Diffraction rings from the BN crucible are also clearly visible under this condition. An ultrabright diffraction spot (shown by the arrow in Figure 3(b)) is from $\{111\}_{\text{fcc}}$ planes, and this spot overlaps with the diffraction ring from BN. This is indeed expected since there are many small austenite grains (at 1153 K (880 °C)) with random orientation on heating just above the Ac_3 temperature. This diffraction conditions are similar to that of powder diffraction and we observe continuous rings. If we assume an average austenite grain size of 10 μm at this temperature, using the estimated irradiated surface area (2.07 mm^2) and penetration depth (16 μm), the estimated number of austenite grains that may be in diffraction condition may be greater than 30,000. However, continued heating above 1153 K to 1516 K (880 °C to 1243 °C) will lead to rapid austenite grain growth, and the average grain size may increase above 130 μm. Under these conditions, only a few (<10) austenite grains are estimated in the ideal diffraction condition within the irradiated volume. Continued growth of austenite grain size will eventually lead to a transition from powder diffraction to single-crystal diffraction conditions. Moreover, our experimental setup does not allow for recording of diffraction from all solid angles (Debye–Scherer cones), which satisfies Bragg's law. As a result, the integrated intensity of austenite at these temperatures will be close to the background levels (Figure 4). This is expected to produce low signal-to-noise ratio (SNR) while analyzing the data from austenite. A rapid change in austenite grain growth (~130 μm) is also supported by the LSCM images to be discussed in Section III–B.

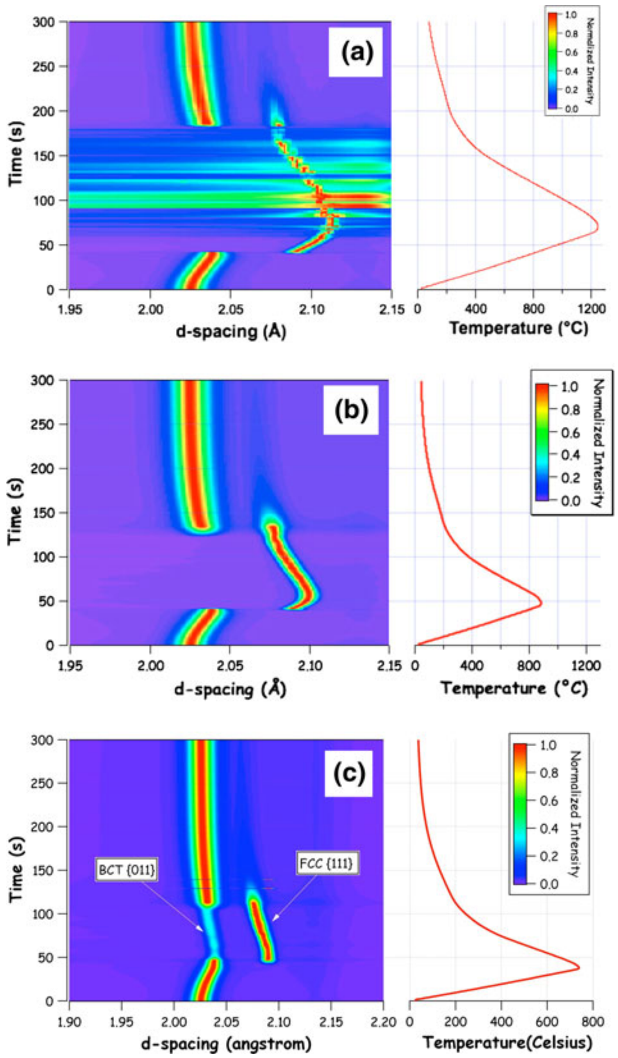

Fig. 4—Overview of the TRXRD data in the image format and associated time and temperature variations are presented here. (*a*) *Data from CGHAZ sample*: Low SNR (<0.3) is observed for austenite diffraction peaks during cooling. SNR is improved after the start of martensite transformation. (*b*) *Data from FGHAZ sample*: High SNR (51.2) is observed in the austenite region throughout the thermal cycle. (*c*) *Data from ICHAZ sample*: The presence of bcc/bct peaks all the time indicates incomplete martensite to austenite transformation (75 pct).

Phase transformations from austenite to martensite were analyzed using TRXRD data. The crystal structure of martensite is body-centered-tetragonal (bct), and the tetragonal distortion (c/a ratio) is related to the carbon concentration. Since the carbon content in BA-160 is low (0.06 wt pct), current experiments cannot distinguish the peak splitting in martensite. Therefore, in this article, martensite data are represented as body-centered-cubic (bcc) structure in all the results. Furthermore, diffraction data from $\{111\}_{\text{fcc}}$ and $\{011\}_{\text{bcc}}$ plates are selected for further analysis. The normalized intensities of $\{111\}_{\text{fcc}}$ and $\{011\}_{\text{bcc}}$ diffraction data in an image format, for all the HAZ samples with corresponding thermal cycles, are shown in Figure 4. In the CGHAZ sample (Figure 4(a)), immediately after the completion of martensite to austenite transformation, the data from $\{111\}_{\text{fcc}}$ show good SNR. As expected from our previous discussions, the SNR reduce significantly (<0.3) when the sample temperature reaches the peak temperature of 1516 K (1243 °C). Interestingly, as soon as the austenite decomposition starts, the SNR of $\{111\}_{\text{fcc}}$ increases to 5.6. This is consistent with the data from Terasaki and Komizo.[23] The preceding increase in SNR is rationalized by the geometrical considerations. On reaching the martensitic start temperature, the first martensitic plate will subdivide the large austenite grain into two major compartments. This will also result in small surface reliefs in the sample. This phenomenon is supported by the LSCM images (Figure 5). As a result, the austenite grains in the diffraction condition increase. With continued cooling, the next set of martensite plates forms and subdivides the austenite grains furthermore. The preceding phenomena will be repeated with continued cooling, and the number of austenite compartments will increase in geometric progression. This leads to a transition of diffraction condition from single crystal to powder diffraction, thereby increasing the SNR. The preceding discussions are consistent with the data obtained from FGHAZ (Figures 4(b) and (c)) and ICHAZ samples. In both cases, the austenite grain size

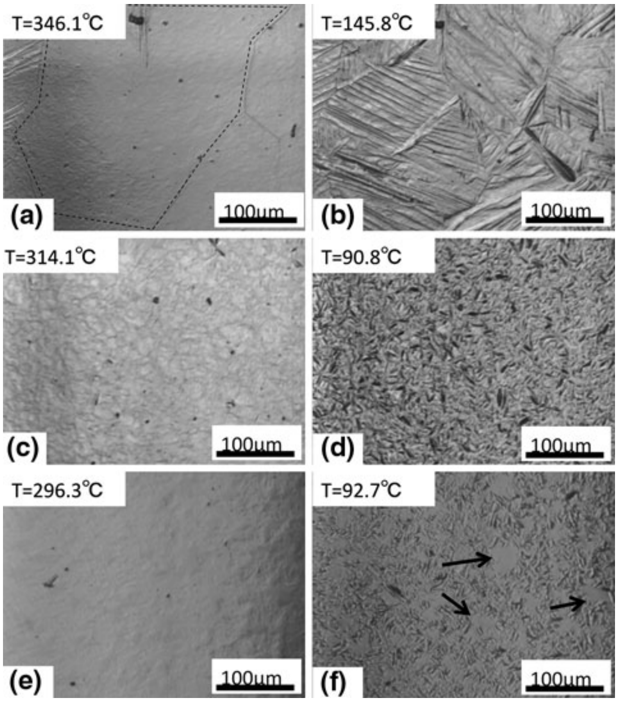

Fig. 5—LSCM images obtained at some typical temperatures during the onset and completion of the austenite-to-martensite transformation are presented. *CGHAZ*: Images from CGHAZ samples show (*a*) large austenite grain size and (*b*) large martensite packets. *FGHAZ*: Images from the FGHAZ show (*c*) fine austenite grains (mottled pattern) and the onset of the first martensite packets (black regions). (*d*) After the completion of transformation, the refinement of the martensite packet size is clear compared to CGHAZ samples. *ICHAZ*: Images from the intercritical HAZ samples showing (*e*) featureless polished surfaces due to lack of clear γ/γ boundaries due to incomplete transformation and the onset of the first martensite plate (dark region). (*f*) After completion of transformation, similar to FGHAZ, refined martensite packet size is observed. Note the temperature correction of 57 deg was made for the above data.

remains lower than 10 μm. As a result, the SNR of austenite diffraction peaks remains at or about 50. It is noteworthy that in case of ICHAZ samples, the transformation to austenite is not complete (Figure 4(c)). On reaching the peak temperature, approximately 25 pct of the original martensite structure is calculated to be present still. Therefore, the austenite grain size is expected to be much smaller than 10 μm.[3]

Careful analyses of the data shown in Figure 4(c) also showed puzzling behavior with reference to the continued increase in volume fraction of austenite during the early stages of the cooling cycle. This behavior was rationalized by recent measurements of the top and bottom surface, which showed a phase lag in temperature between these locations when the large change was set in the course of thermal cycle.[24] Nevertheless, these recent measurements also confirmed that the measured peak temperatures are indeed the same and allowed us to compare the results from different HAZ samples. Since our focus is martensitic transformation characteristics, a temperature correction has to be made to analyze these TRXRD and LSCM data. The martensite start temperature derived from dilatation analysis for the CGHAZ sample was found to be 620 K (347 °C), which is 330 K (57 °C) higher than that observed in the current hybrid technique. Previous research showed that M_s measurements are accurate with the dilatation technique.[3] Therefore, the current investigation assumed a constant temperature gradient of 57 °C from the sample surface to the bottom for subsequent analyses and results. The preceding corrections are made for interpretation of all TRXRD and LSCM data and are specifically called out in all the figures.

B. *LSCM Observations*

Figure 5 shows snapshots of LSCM images before and during austenite-to-martensite transformation during cooling for all HAZ samples. It is noteworthy that the images in LSCM are attained by a change in surface topology. The austenite (γ-γ) grain boundaries are imaged due to surface grooving. In the CGHAZ sample (Figure 5(a)), large austenite grains (~130 μm) can be seen at the onset of martensite transformation at 619 K (346 °C). In this image, fresh martensite packets can be seen adjacent to γ-γ grain boundaries (left side of the image). The martensite packets are imaged in the LSCM technique due to the surface relief that occurs during displacive transformation of austenite to martensite.[25] In this work, we cannot delineate individual martensite plate growth, because the plates form in less than 10^{-7} s,[25] which is smaller than the LSCM time resolution of 0.03 seconds. The LSCM image obtained at 419 K (146 °C) shows more or less completion of austenite-to-martensite transformation. Many variants of martensite plates can also be seen. In addition, one can conclude that the martensite packets and blocks (Figure 5(b)) are larger in comparison to the data from other samples to be presented subsequently.

In the FGHAZ sample, austenite grains (Figure 5(c)) with an average grain size of 10 μm are observed at 587 K (314 °C). Interestingly, no martensite transformation can be discerned from the images at this temperature. In contrast, the LSCM images from CGHAZ samples showed the onset of martensitic transformation at 619 K (346 °C). Sequential analyses of LSCM images from these samples showed dramatic reduction in martensite packet sizes. Fine martensite packets and blocks are also evident from the LSCM image at 364 K (91 °C), when the transformation is nearly complete (Figure 5(d)).

In the ICHAZ sample, the LSCM did not show clear γ-γ grain boundaries (Figure 5(e)). This is indeed expected, because the austenite-to-martensite transformation is not complete on reaching the peak temperature. TRXRD data showed that, on heating to peak temperature, newly formed austenite and untransformed martensite must coexist. Since the surface of these samples is in the polished condition, the original martensite boundaries (α/α) cannot be visualized. The newly formed austenite may lead to the formation of α-γ interphase boundaries, as well as γ-γ grain boundaries. On cooling to 569 K (296 °C), the first martensite packet formation was imaged at a temperature of 569 K (296 °C). After cooling below 366 K (93 °C), LSCM images show completion of martensite transformation

(Figure 5(f)). These images show a fine martensite packet, as well as the original featureless white regions (marked by arrows in Figure 5(f)). These regions are interpreted as the original martensite regions that have not been transformed on heating.

C. *Dilatometry Measurements*

Phase transformation strains were also measured using a dilatometer while subjected to different HAZ thermal simulations. A typical dilatation curve for the FGHAZ sample is shown in Figure 6. As the specimen is heated (at 20 °C·s^{-1}) from room temperature, the relative radius change increases with a nearly constant positive slope dictated by the coefficient of thermal expansion of ferrite. On reaching the Ac_1 (933 K (660 °C)), temperature martensite transforms to austenite, which is associated with a contraction. The dilatation curve becomes linear at Ac_3 (1013 K (740 °C)), due to the completion of transformation to austenite. The thermal expansion coefficient for martensite ($1.088 \pm 0.001 \times 10^{-5}$) and austenite ($2.375 \pm 0.001 \times 10^{-5}$) can be calculated from these curves. Next, the volume fraction of austenite and martensite can be calculated by geometric methods developed by Eldis[26] and Babu.[27] The same approach is used in the martensite fraction calculation during cooling in Figure 7(b).

D. *Discussion on M_s and Martensite Transformation Rates*

The data shown in Figure 4 were analyzed further by fitting a Gaussian peak to $\{111\}_{\text{fcc}}$ and $\{011\}_{\text{bcc}}$ diffraction peaks of the form[13]

$$I = I_0 \exp\left[\left(\frac{d - d_0}{w}\right)^2\right] \qquad [1]$$

where I is the observed intensity as a function of interplanar spacing, I_0 is the intensity for a given mean interplanar spacing d_0, and w is given by the Gaussian peak width. After peak fitting, the areas under $\{111\}_{\text{fcc}}$ and $\{011\}_{\text{bcc}}$ peaks are integrated. The phase volume fraction was derived by using the direct comparison method considering structure factor, multiplicity factor, Lorentz polarization, and temperature factor.[28] Martensite fraction (f_m) as a function of temperature is plotted in Figure 7(a). The M_s values for CGHAZ, FGHAZ, and ICHAZ are 622 K, 584 K, and 566 K (349 °C, 311 °C, and 293 °C), respectively. This reveals a reduction of M_s temperature with a reduction in austenite grain size. This result is in agreement with the measured M_s by Yang and Bhadeshia using the dilatometric technique.[29] From Figure 7(a), it can be seen that the martensite fraction has a nearly linear relationship with temperature when $0.1 < f_m < 0.5$. By fitting a linear curve through martensite fraction ($0.1 < f_m < 0.5$) as a function of temperature, the transformation rate df_m/dT was calculated for all the data shown in Figure 7(a). The magnitudes of df_m/dT are found to be 0.033 °C^{-1}, 0.018 °C^{-1}, and 0.012 °C^{-1} for CGHAZ, FGHAZ, and ICHAZ, respectively. The preceding calculations also suggest that an increase in austenite grain size also promotes the transformation rate. It is realized that in our data analyses, only one pair of diffraction peaks ($\{111\}_{\text{fcc}}$ and $\{011\}_{\text{bcc}}$) is considered to derive the martensite volume fraction. For FGHAZ and ICHAZ, the result is accurate since the prior austenite grain size is small (<10 μm). However, for CGHAZ,

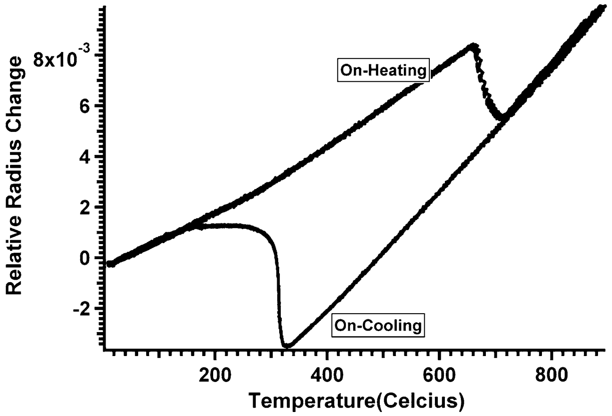

Fig. 6—Relative radius change *vs* temperature obtained from FGHAZ samples showing on-heating ($\alpha' \rightarrow \gamma$) and on-cooling ($\gamma \rightarrow \alpha'$) transformations.

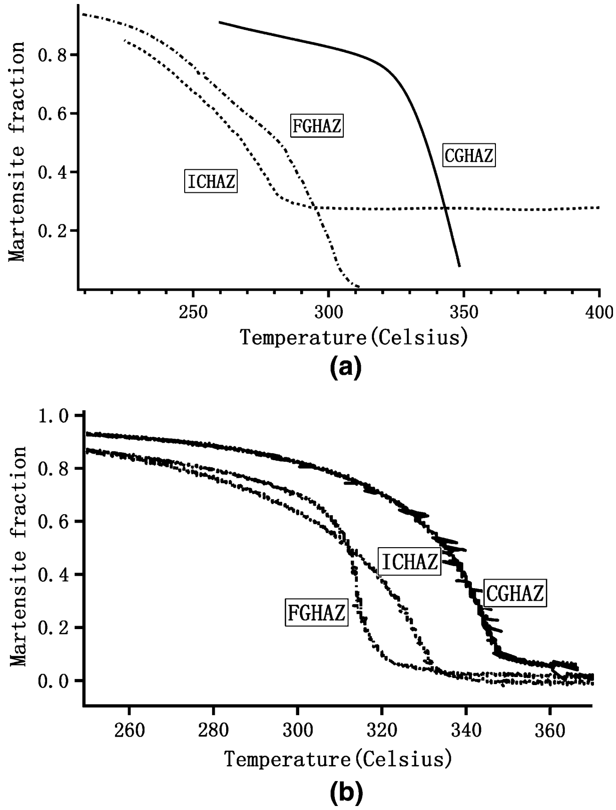

Fig. 7—Measured fraction of martensite as a function of temperature on cooling from different techniques. (*a*) *TRXRD data*: This is determined by the direct comparison method using {011}-bcc and {111}-fcc peaks. Note the temperature correction of 57 deg was made for the TRXRD data. (*b*) *Gleeble dilatation measurement*: This is determined by the geometric method, which assumes linear dilatation in the pure γ- and α'-phase fields.

since the prior austenite grain is large (>130 μm), the analyzed volume has less than 10 austenite grains. This small number may give a less accurate result on martensite volume fraction. We believe that transmission type three-dimensional X-ray diffraction methodology with large beam size may indeed improve these results and is indeed the focus of the future work.[30]

To reconfirm the preceding result, the dilatometry data are also analyzed (Figure 7(b)) further. Due to the uncertainty of the exact temperature in the TRXRD data, these comparisons are made in terms of trends only. First, the dilatation data from CGHAZ and FGHAZ regions are discussed. The CGHAZ sample shows the highest M_s (621 K (348 °C)) compared to that of the FGHAZ (604 K (331 °C)). Thus, the data reconfirm the trend of decreasing M_s with a decrease in austenite grain size, in both techniques. However, it is clear that there is a discrepancy in measurements with respect to ICHAZ (M_s = 604 K (331 °C)) from TRXRD and dilatometric data. The following paragraph attempts to explain this discrepancy based on the inability to control the peak temperature with reference to Ac_1 and Ac_3 transformation temperatures during TRXRD measurements and the resulting difference in extent of transformation to austenite. During dilatometry experiments, the ICHAZ sample shows nearly complete (99 pct) transformation of martensite to austenite on reaching the peak temperature of 1011 K (738 °C). However, in TRXRD data, the transformation to austenite is only 75 pct complete (Figure 7(a)). Therefore, on reaching the peak temperature, the austenite is expected to have higher carbon concentration. According to thermodynamic calculation using THERMO-CALC** (with TCFE5 database),[31] the carbon concentration of ferrite (or original martensite) in equilibrium with austenite at 933 K (660 °C) will be 0.0007 wt pct. Taking 25 pct as the untransformed martensite region, the carbon concentration in the remaining (75 pct) austenite will be 0.08 wt pct. This is indeed higher than nominal carbon concentration (0.06 pct) of the steel. Therefore, the M_s temperature will reduce further due to a reduction in driving force for austenite to martensite on cooling to low temperature. According to Beres's empirical formula,[32] an increase in carbon concentration by 0.02 pct will reduce M_s by 13.3 °C.

In the next set of comparisons, the calculated transformation rates (df_m/dT) from dilatation data are compared. The absolute values of df_m/dT at ($0.1 < f_m < 0.5$) are 0.032 °C^{-1} and 0.055 °C^{-1} for CGHAZ and FGHAZ, respectively. This trend is indeed inconsistent between the two techniques. Currently, we cannot rationalize these inconsistencies. Three possible hypotheses are put forward. (1) The inconsistencies can be due to stochastic variations of prior austenite grain in different samples due to small variations in peak temperature. When the peak temperature is high, the austenite grain size is not sensitive to small variation in peak temperature. However, if the peak temperature is slightly above Ac_1, a small change in peak temperature will result in large differences in austenite grain size. (2) These inconsistencies also can be due to differences in the sampled volume in TRXRD and dilatation techniques. TRXRD characterizes the martensite transformation in a localized surface area of the sample. Sectioning effect and free surface may cause the transformation kinetics to be largely different. Dilatation, on the other hand, is a volumetric measurement and averages many grains. Martensite transformation kinetics derived from dilation shows the average of the sample. (3) As discussed earlier, the extent of martensite-to-austenite transformation on heating may dictate the carbon concentration of freshly formed austenite. A change in austenite carbon concentration will also change the $\gamma \rightarrow \alpha'$ transformation rates.

Since the data from CGHAZ samples were consistent in both measurement techniques, these data were compared with the published martensite kinetics model. Yang and Bhadeshia[29] derived the equation to describe martensite transformation kinetics in steels:

$$f_m = 1 - \exp\left\{-m \cdot \ln\left\{1 + aV_\gamma\left(\exp\left\{b\left(M_S^0 - T\right)\right\} - 1\right)\right\}\right\} \qquad [2]$$

In the preceding equation, m is the martensite block aspect ratio (0.05), and a (1 mm^{-3}) and b (0.2689) are empirically fitted parameters. The V_γ is the average volume of austenite grain before the onset of martensite transformation. The M_s^0 is the highest temperature at which martensite can form and can be calculated by considering the thermodynamics and stored energy of martensite (~700 J/mol). Thermodynamic (TCFE5 database in THERMO-CALC) models were used to calculate the M_s^0 of BA-160 steel to be 669 K (396 °C). The predicted martensite fraction for the CGHAZ condition by Eq. [2] was compared with experimental measurements (Figure 8) from TRXRD and dilatometry. It is interesting that the rate of martensite fraction is almost identical for both TRXRD and dilatometry when the extent of transformation is less than 0.6. However, the predicted martensite fraction by Eq. [2] shows a sluggish transformation rate. It is quite possible to modify the empirical parameters (a and b) to fit the data. However, we believe these parameters need to be derived by leveraging the spatial morphology of martensite packets that are derived from LSCM images. Specific focus needs to be put on extending Eq. [2], which relies on geometric progression to consider the stabilization of austenite[33] at a given subdivision. Some of the emerging research in analyzing the microstructural evolution in steels through fractal theories can be leveraged for the same.[34]

E. *Challenges in Hybrid Technique*

The main challenge is related to the uncertainty in temperature measurements in the hybrid system. Such effects were not observed in earlier work due to

---

**THERMO-CALC is a trademark of Thermo-Calc, Stockholm.

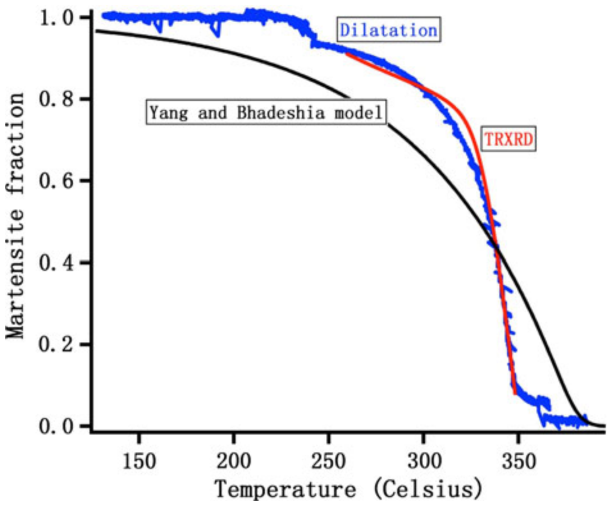

Fig. 8—Martensite fraction *vs* temperature values on cooling for samples with 130-μm prior austenite grain size derived from prediction (Eq. [2]) and experimental (TRXRD and dilatometry) measurements are compared. Note the temperature correction of 57 deg was made for the TRXRD data.

relatively slow heating rates.[18] Recently, Sharma *et al.* developed a furnace for synchrotron-based *in-situ* measurements.[35] In this work, the authors discussed methodologies to control temperature in detail. However, their system does not rely on any optical microstructure analyses similar to the current hybrid system. Our ongoing research focuses on redesigning the sample holder to allow for comprehensive measurements of temperature on the surface without interfering with the diffraction geometry. In addition, *in-situ* measurements of inclusion locations on the surface of the sample can be leveraged through image analyses. These positional measurements can be used to calculate thermal expansion coefficients of the sample in the pure phase region (austenite or ferrite), through which the actual temperature of the surface could be corrected.

F. *Summary and Conclusions*

A hybrid *in-situ* technique, which combines a TRXRD method using synchrotron and a laser scanning confocal microscope, was used to track microstructure evolution in the HAZ of BA-160 steels. The kinetics of phase transformations during thermal cycling with different peak temperatures was tracked at a 0.3-second time resolution. The data were compared with dilatometric measurements. The measurements from hybrid TRXRD and LSCM showed the following.

1. SNR of austenite diffraction peaks increased with a decrease in austenite grain size.
2. Reduction in martensite start temperature was observed with small austenite grain sizes.
3. Significant changes in transformation rates were also observed with different austenite grain sizes.
4. LSCM analyses showed refinement of martensite structure with a reduction in austenite grain size.
5. Predicted martensite fraction *vs* temperatures show similar trends as that of a published theoretical model; however, the magnitude of predicted rates is lower than that of experimental measurements.

Comparison of the preceding measurements with dilatometric measurements revealed some difficulties. The volumetric (dilatometer) and surface (synchrotron and LSCM) measurements show inconsistent quantitative values in tracking kinetics of martensite transformation (df_m/dT). The highest martensite transformation rate is observed with austenite grain sizes of 130 μm in synchrotron X-ray diffraction. However, dilation analyses show the fastest transformation in the sample with austenite grain size below 10 μm.

ACKNOWLEDGMENTS

The authors acknowledge the financial support from the United States Office of Naval Research (Washington, DC). In addition, encouragement and support of the program managers, Drs. J. Christodoulou and W. Mullins in this research, are also appreciated. Xinghua Yu was partially supported by the IMI Program of the National Science Foundation under Award No. DMR 0843934 for his travel to Spring-8 facilities to perform *in-situ* phase transformation (LSCM and TRXRD) measurements.

REFERENCES

1. A. Saha and G.B. Olson: *J. Comput. Aided Mater. Des.*, 2007, vol. 14, pp. 177–200.
2. A. Saha and G.B. Olson: *J. Comput. Aided Mater. Des.*, 2007, vol. 14, pp. 201–33.
3. X. Yu, J.L. Caron, S.S. Babu, J.C. Lippold, D. Isheim, and D.N. Seidman: *Acta Mater.*, 2010, vol. 58, pp. 5596–5609.
4. X. Yu, J.L. Caron, S.S. Babu, J.C. Lippold, D. Isheim, and D.N. Seidman: *Metall. Mater. Trans. A*, DOI:10.1007/s11661-011-0707-y.
5. S. Morito, H. Yoshida, T. Maki, and X. Huang: *Mater. Sci. Eng. A*, 2006, vol. 438, pp. 237–40.
6. H. Yin, T. Emi, and H. Shibata: *Acta Mater.*, 1999, vol. 47, pp. 1523–35.
7. A.M. Elwazri, P. Wanjara, M. Brochu, and S. Yue: *Microsc. Microanal.*, 2005, vol. 11, pp. 634–35.
8. D.J. Phelan, M.H. Reid, and R.J. Dippenaar: *Microsc. Microanal.*, 2005, vol. 11, pp. 670–71.
9. N. Oku, K. Asakura, J. Inoue, and T. Koseki: *Trends in Welding Research, Proc. 8th Int. Conf.*, ASM International, Materials Park, OH, 2009, pp. 272–76.
10. Y. Komizo and H. Terasaki: *Sci. Technol. Weld. Join.*, 2011, vol. 16, pp. 56–60.
11. Y. Komizo and H. Terasaki: *Sci. Technol. Weld. Join.*, 2011, vol. 16, pp. 61–67.
12. J.W. Elmer, J. Wong, and T. Ressler: *Scripta Mater.*, 2000, vol. 43, pp. 751–57.
13. S.S. Babu, J.W. Elmer, J.M. Vitek, and J.M. David: *Acta Mater.*, 2002, vol. 50, pp. 4763–81.
14. J. Wong, Ressler, and J.W. Elmer: *J. Synchrotron Rad.*, 2003, vol. 10, pp. 154–67.
15. S.S. Babu, E.D. Specht, S.A. David, E. Karapetrova, P. Zschack, M. Peet, and H.K.D.H. Bhadeshia: *Metall. Mater. Trans. A*, 2005, vol. 36A, pp. 3281–89.
16. H.J. Stone, M.J. Peet, H.K.D.H. Bhadeshia, P.J. Withers, S.S. Babu, and E.D. Specht: *Proc. R. Soc. A*, 2009, vol. 464, pp. 1009–27.
17. S.E. Offerman, N.H. van Dijk, J. Sietsma, S. Grigull, E.M. Lauridsen, L. Margulies, H.F. Poulsen, M.T. Rekveldt, and S. van der Zwaag: *Science*, 2002, vol. 298, pp. 1003–05.
18. Y. Komizo and H. Terasaki: *Sci. Technol. Weld. Join.*, 2011, vol. 16, pp. 79–86.

19. H.K.D.H. Bhadeshia: *J. Phys. Coll. C4,* 1982, vol. 43, pp. C-435–441.
20. C. Broennimann, E.F. Eikenberry, B. Henrichn, R. Horisberger, G. Huelsen, E. Pohl, B. Schmitt, C. Schulze-Briese, M. Suzuki, T. Tomizaki, H. Toyokawa, and A. Wagner: *J. Synchrotron Rad.*, 2006, vol. 13, pp. 120–30.
21. A.P. Hammersley, S.O. Svensson, M. Hanfland, A.N. Fitch, and D. Häusermann: *High Press. Res.*, 1996, vol. 14, pp. 235–48.
22. A.P. Hammersley: ESRF Internal Report No. ESRF97HA02A, ESRF, Grenoble, Cedex, France, 1997.
23. H. Terasaki and Y. Komizo: *Scripta Mater.*, 2011, vol. 64, pp. 29–32.
24. H. Terasaki: JWRI, Osaka University, Osaka, unpublished research, 2011.
25. H.K.D.H. Bhadeshia and R.W.K. Honeycombe: *Steels: Microstructure and Properties*, Butterworth-Heinemann, Oxford, United Kingdom, 2006.
26. G. Eldis: in *Hardenability Concepts with Applications to Steel*, AIME, New York, NY, 1978, pp. 126–57.
27. S.S. Babu: Ph.D. Thesis, University of Cambridge, Cambridge, United Kingdom, 1992.
28. B.D. Cullity: *Elements of X-Ray Diffraction*, Addison-Wesley Publishing Inc., Reading, MA, 1978.
29. H.S. Yang and H.K.D.H. Bhadeshia: *Scripta Mater.*, 2007, vol. 60, pp. 493–95.
30. T.H. Kannengiesser, S.S. Babu, Y. Komizo, and A.J. Ramirez, eds., *In-Situ Studies with Photons, Neutrons and Electrons Scattering*, 1st ed., Springer, New York, NY, 2010.
31. J.O. Andersson, T. Helander, L. Höglund, P.F. Shi, and B. Sundman: *CALPHAD*, 2002, vol. 26, pp. 273–312.
32. L. Beres, Z. Beres, and W. Irmer: *Weld. Cutt.*, 1994, vol. 8, pp. 128–30.
33. E. Hornbogen: *Int. Mater. Rev.*, 1989, vol. 34, pp. 277–96.
34. M. Tarafder, I. Chattoraj, S. Tarafder, and M. Nasipuri: *Mater. Sci. Technol.*, 2009, vol. 25, pp. 542–48.
35. H. Sharma, A. Wattjes, M. Amirthalingam, T. Zuidwijk, N. Geerlofs, and S.E. Offerman: *Rev. Scientific Instrum.*, 2009, vol. 80, p. 123301.